Available online at www.sciencedirect.com
SCIENCE DIRECT
Journal of Power Sources 157 (2006) 507–514
JOURNAL OF POWER SOURCES
www.elsevier.com/locate/jpowsour

Effects of ball-milling on lithium insertion into multi-walled carbon nanotubes synthesized by thermal chemical vapour deposition

JiYong Eom, DongYung Kim, HyukSang Kwon *

Department of Materials Science & Engineering, Korea Advanced Institute of Science & Technology, 373-1, Guseong-dong, Yuseong-gu, Daejon 305-701, Republic of Korea

Received 17 May 2005; accepted 16 August 2005
Available online 7 December 2005

Abstract

The effects of ball-milling on Li insertion into multi-walled carbon nanotubes (MWNTs) are presented. The MWNTs are synthesized on supported catalysts by thermal chemical vapour deposition, purified, and mechanically ball-milled by the high energy ball-milling. The purified MWNTs and the ball-milled MWNTs were electrochemically inserted with Li. Structural and chemical modifications in the ball-milled MWNTs change the insertion–extraction properties of Li ions into/from the ball-milled MWNTs. The reversible capacity (C_{rev}) increases with increasing ball-milling time, namely, from 351 mAh g^{-1} ($Li_{0.9}C_6$) for the purified MWNTs to 641 mAh g^{-1} ($Li_{1.7}C_6$) for the ball-milled MWNTs. The undesirable irreversible capacity (C_{irr}) decreases continuously with increase in the ball-milling time, namely, from 1012 mAh g^{-1} ($Li_{2.7}C_6$) for the purified MWNTs to 518 mAh g^{-1} ($Li_{1.4}C_6$) for the ball-milled MWNTs. The decrease in C_{irr} of the ball-milled samples results in an increase in the coulombic efficiency from 25% for the purified samples to 50% for the ball-milled samples. In addition, the ball-milled samples maintain a more stable capacity than the purified samples during charge–discharge cycling.

Keywords: Multi-walled carbon nanotubes; Capacity; Chemical vapour deposition; Grinding; Electrochemical properties; Lithium-ion battery

1. Introduction

Carbon nanotubes (CNTs), multi-walled carbon nanotubes (MWNTs) and single-walled carbon nanotubes (SWNTs) have received much attention as Li insertion host materials for high-energy Li-ion rechargeable batteries. MWNTs prepared by various synthesis conditions [1–3] and thermal oxidation treatments [4–6] have exhibited reversible capacities of 80–640 mAh g^{-1} ($Li_{0.2}C_6 \sim Li_{1.7}C_6$). Lithium reversible capacities of raw SWNTs and purified SWNTs have been reported to be 450–600 mAh g^{-1} ($Li_{1.2}C_6 \sim Li_{1.6}C_6$) [7,8], and to increase to 790 and 1000 mAh g^{-1} ($Li_{2.1}C_6$ and $Li_{2.7}C_6$) on either mechanical ball-milling [9] or chemical etching [10,11]. Although the Li reversible capacity of CNTs is higher than that of graphite, viz., 372 mAh g^{-1} (LiC_6), the irreversible capacity is still very high. Therefore, anodes using CNTs that have been reported previously present a very low coulombic efficiency of 30%.

High-energy ball-milling techniques have long been employed for the production of composite metallic powders with fine, controlled microstructures [12]. Recently, this technique was used to study the effect of mechanical ball-milling on Li insertion into sugar carbons that have a microporous structure [13]. The authors found that the graphene layers initially become more stacked, the nanoscopic or microscopic pores are rapidly eliminated, and the number of macropores or mesopores increases. Further, the Li reversible capacity of the ball-milled sugar carbon increased more than the irreversible capacity, and thus gave a greater coulombic efficiency. Therefore, it is concluded that the Li reversible capacity and the coulombic efficiency of MWNTs can also be increased by the high energy ball-milling.

In this study, MWNTs have been subjected to high-energy ball-milling. The structural characteristics and the surface functional groups of the processed MWNTs have been investigated together their effect on Li insertion.

* Corresponding author. Tel.: +82 42 869 3326; fax: +82 42 869 3310.
E-mail address: hskwon@kaist.ac.kr (H.S. Kwon).

0378-7753/$ – see front matter © 2005 Elsevier B.V. All rights reserved.
doi:10.1016/j.jpowsour.2005.08.024

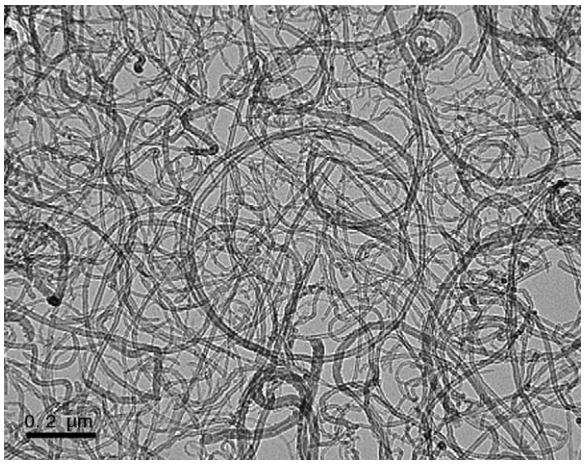

Fig. 1. Transmission electron micrographs of purified MWNTs by an acidic treatment followed by a gas-phase oxidation process.

2. Experimental

2.1. Mechanical ball-milling of MWNTs

The MWNTs were synthesized on supported catalysts by thermal chemical vapour deposition (CVD) and then purified by an acidic treatment followed by a gas-phase oxidation process [14,15]. The final purified products consisted of 95% MWNTs with a length of over 10 μm and a diameter of about 10–20 nm, as shown in Fig. 1.

The purified MWNTs (50 mg samples) were ball-milled in a stainless-steel vial by the impact mode of a stainless-steel ball in air. All the ball-milled samples were dried at 150 °C for 5 h in a 5×10^{-6} Torr vacuum before using.

2.2. Electrochemical test of Li/MWNTs cells

Charge–discharge tests of Li/MWNTs cells was performed under a galvanostatic mode using a WBCS 3000 (WonATech©) system. The cells were discharged (insertion) and charged (extraction) at a constant current of 50 mA g^{-1} between 0 and 3 V. Cyclic voltammetry of Li/MWNTs cells was performed at a constant scan rate of 0.1 mV s^{-1} between 0 and 3 V.

The cell for charge–discharge and the cyclic voltammetry tests used Li foil as the anode and a MWNTs film as the cathode. The MWNTs electrodes were prepared by coating slurries consisting of MWNTs (85 wt.%) with acetylene carbon black (5 wt.%) and poly(vinylidene fluoride) (PVdF) (10 wt.%) as a binder dissolved in 1-methyle-2-pyrrolidinone (NMP) solution on a stainless-steel substrate. All the MWNTs electrodes were dried for 5 h at 150 °C in a 5×10^{-6} Torr vacuum. After drying, the weight of each sample was about 2–4 mg. The Li/MWNTs cells were assembled as coin types in an argon-filled glove box. A polypropylene filter soaked with a liquid electrolyte (Merck©) of 1 M $LiPF_6$ dissolved in a 1:1 volume ratio of ethylene carbonate (EC) and diethyl carbonate (DEC) was placed between the anode and the cathode.

3. Results and discussion

3.1. Structure of ball-milled MWNTs

Scanning electron micrographs of the purified MWNTs and the ball-milled MWNTs are shown in Fig. 2. It is seen that the purified MWNTs have a uniform and porous 'spaghetti'-type structure in which the individual MWNTs are clearly visible. By contrast, ball-milled MWNTs have a densely-packed structure in which the individual MWNTs are fractured and flattened with increase in the ball-milling time.

X-ray diffraction patterns of the purified MWNTs and the MWNTs ball-milled for 60 min are shown in Fig. 3. The intensity of the (0 0 2) and (1 0 1) diffraction peaks for the ball-milled MWNTs are smaller and broader than those for the purified MWNTs. The d(0 0 2) spacing, or the distance between the graphene layers, and the d(1 0 1) spacing, or the distance between the carbon atoms on basal plane of the purified MWNTs, is calculated to be 3.44 and 2.12 Å, respectively. For MWNTs ball-milled for 60 min, the (0 0 2) and (1 0 1) diffraction peaks shift slightly to a higher angle, and hence the d(0 0 2) and d(1 0 1) spacing decreases to 3.43 and 2.09 Å, which indicates that the structure of the MWNTs is disordered and the graphene layers of MWNTs are flattened slightly by high-energy ball-milling.

Transmission electron micrographs of the ball-milled MWNTs are given in Fig. 4. These demonstrate that the average length of the MWNTs is reduced to about 0.2 μm after ball-milling for 60 min. The ball-milled MWNTs have a structure with opened ends due to fracture of the individual MWNTs by the ball-milling, as shown in Fig. 4(b).

Raman spectra for the purified MWNTs and the ball-milled MWNTs are presented in Fig. 5. Raman-active vibrational modes associated with MWNTs and disordered carbon are observed in all the samples. The ratio of the total integrated intensity of the disordered carbon mode (around 1350 cm^{-1}) to that of the MWNTs mode (around 1600 cm^{-1}) is increased by ball-milling. This indicates that ball-milling results in a significant increase in the intensity of the disordered carbon mode with broadening of the MWNTs peak, and suggests that MWNTs are being converted into disordered/amorphous carbon.

3.2. Charge–discharge characteristics of ball-milled MWNTs

The charge–discharge characteristics for insertion and extraction of Li ions into/from purified MWNTs and ball-milled MWNTs are displayed in Fig. 6. The reversible capacity (C_{rev}) is defined as the first charge capacity, while the irreversible capacity (C_{irr}) is defined as the difference between the first discharge and charge capacities. The change in C_{rev} and C_{irr}, as well as the coulombic efficiency of the ball-milled MWNTs, are given in Fig. 7 as a function of the ball-milling time. For the purified MWNTs, the C_{rev} is 351 mAh g^{-1} ($Li_{0.9}C_6$), whereas the C_{irr} is 1012 mAh g^{-1} ($Li_{2.7}C_6$) compared with the C_{rev}. The C_{rev} of the ball-milled MWNTs increases with increase in the ball-milling time, i.e., from 351 mAh g^{-1} ($Li_{0.9}C_6$) for the purified MWNTs to 641 mAh g^{-1} ($Li_{1.7}C_6$) after ball-milling for

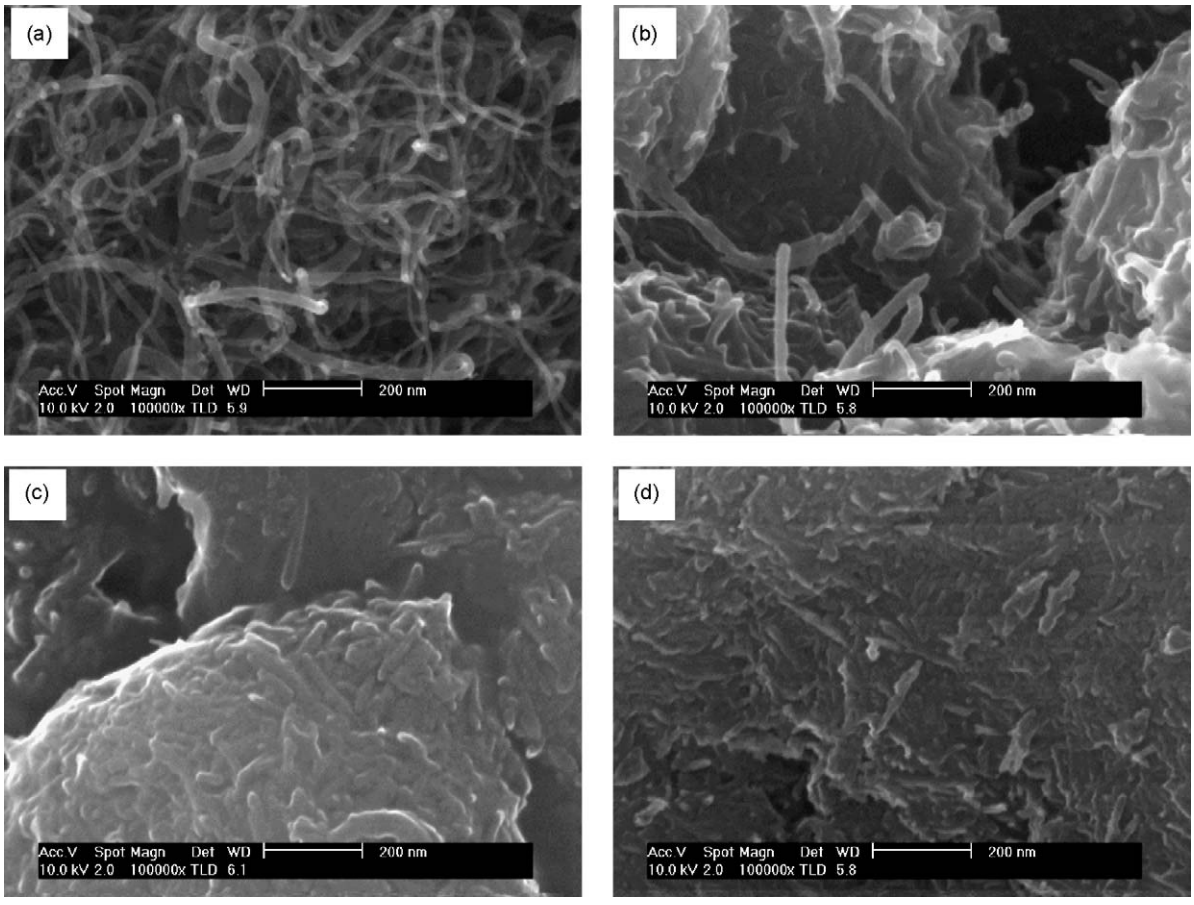

Fig. 2. Scanning electron micrographs of (a) purified MWNTs and ball-milled MWNTs for (b) 10; (c) 60; and (d) 120 min.

60 min. After further ball-milling for 120 min, however, the C_{rev} decreases slightly to 560 mAh g^{-1} ($Li_{1.5}C_6$). The C_{irr} of the ball-milled MWNTs decreases continuously with increase in ball-milling time from 1012 mAh g^{-1} ($Li_{2.7}C_6$) for the purified MWNTs to 518 mAh g^{-1} ($Li_{1.4}C_6$) after ball-milling for 120 min. Therefore, the coulombic efficiency of the ball-milled MWNTs increases continuously with increase in ball-milling time from 26% for the purified MWNTs to 52% after ball-milling for 120 min, as shown in Fig. 7(b). The charge–discharge characteristics for several samples taken from different batches were measured under the same conditions. There is a small deviation in capacity of about ±30 mAh g^{-1}.

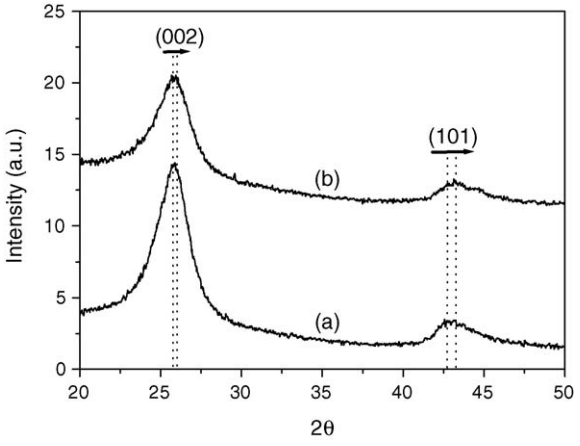

Fig. 3. X-rays diffraction patterns of (a) purified MWNTs and (b) MWNTs ball-milled for 60 min. All samples were contained in a glass capillary tube and then measured using Cu Kα of 1.54 Å at 40 kV in the transmission mode.

The voltage plateau at 0.8 V that appears on the first discharge curves shown in Fig. 6 has been attributed to the decomposition of electrolyte and the formation of a solid electrolyte interface (SEI) on the surface of the MWNTs [16–18] that result in a large C_{irr} for the MWNTs [2,4,5]. The duration of the voltage plateau at 0.8 V is proportional to the surface area of the MWNTs on which the SEI is formed. Therefore, the large surface area of the MWNTs is responsible for the observed large C_{irr}. The voltage plateau at 0.8 V in the first discharge curve for the purified MWNTs is longer than that for the ball-milled MWNTs. This indicates indicating that the C_{irr} of the purified MWNTs is larger than that of the ball-milled MWNTs.

The Brunauer–Emmett–Teller (BET) specific surface area and the pore volume and diameter of the purified MWNTs and the ball-milled MWNTs are shown in Fig. 8 as a function of the ball-milling time. The BET specific surface area in Fig. 8(a) increases with ball-milling time due to the increase in the opened ends and also to the shortened length by fracture of the ball-milled MWNTs. By contrast, the pore volume and diameter of the ball-milled MWNTs abruptly decreases with ball-milling, as shown in Fig. 8(b). This suggests that the ball-milled MWNTs

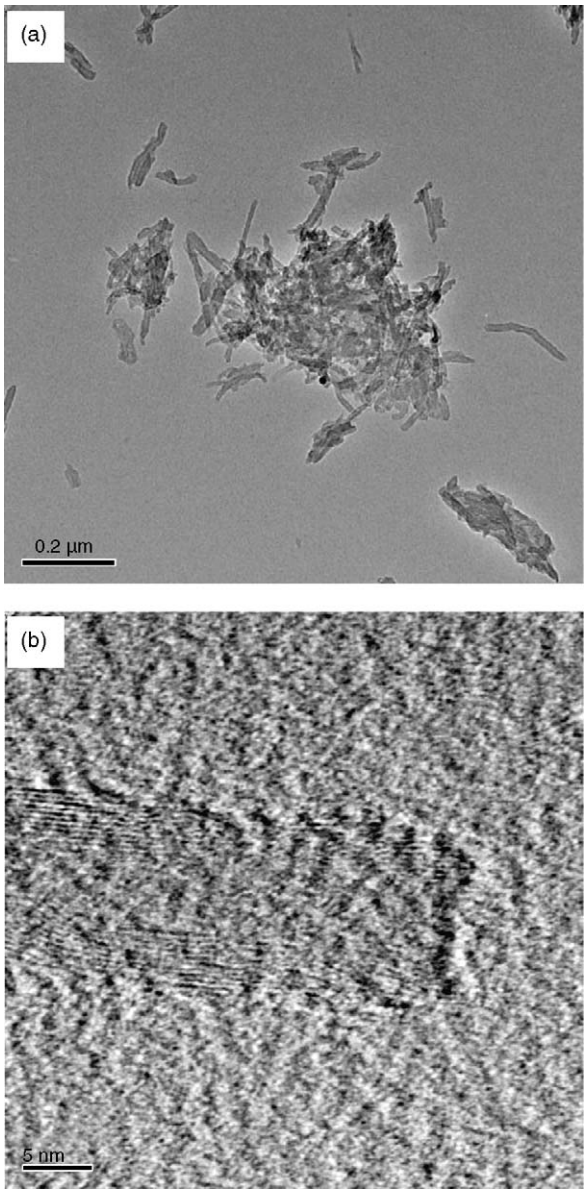

Fig. 4. Transmission electron micrographs of (a) MWNTs ball-milled for 60 min and (b) open (fractured) end of ball-milled MWNTs.

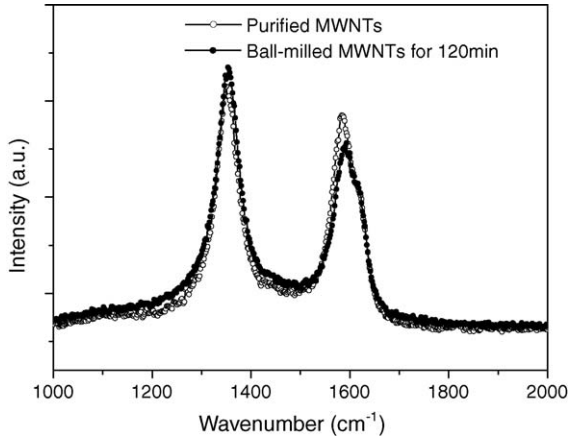

Fig. 5. Raman spectra of purified MWNTs and MWNTs ball-milled for 120 min. Data collected using Ar ion laser of 514.5 nm and micro-Raman spectrometer with CCD detector at room temperature.

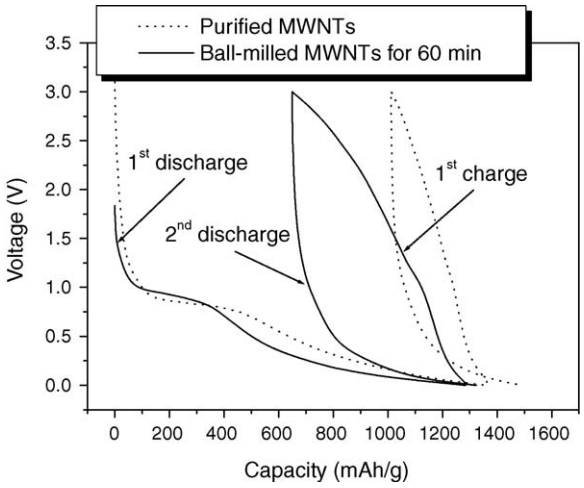

Fig. 6. Charge–discharge curves of Li insertion/extraction into/from purified MWNTs and MWNTs ball-milled for 60 min. The Li/MWNTs cells were discharged (insertion) and charged (extraction) under a galvanostatic mode at a constant current of 50 mA g^{-1} between 0 and 3 V.

have a densel packed structure due to fracture and elattening of the individual MWNTs with ball-milling. The increase in a packing density of the ball-milled MWNTs is believed to be the reason for the reduction in C_{irr} observed in the ball-milled

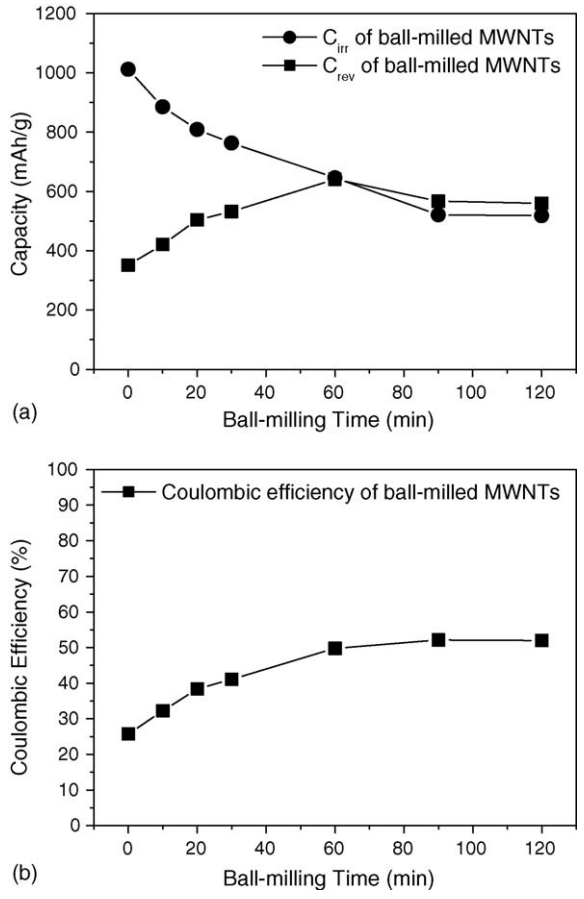

Fig. 7. (a) Change in reversible capacity (C_{rev}) and irreversible capacity (C_{irr}); and (b) coulombic efficiency of ball-milled MWNTs as function of ball-milling time.

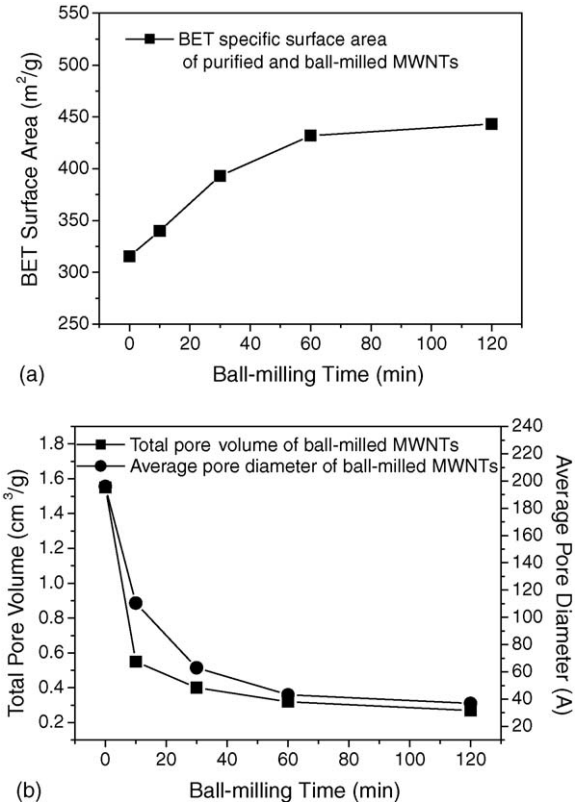

Fig. 8. (a) BET specific surface area and (b) pore volume and diameter of purified MWNTs and ball-milled MWNTs as function of ball-milling time measured using nitrogen.

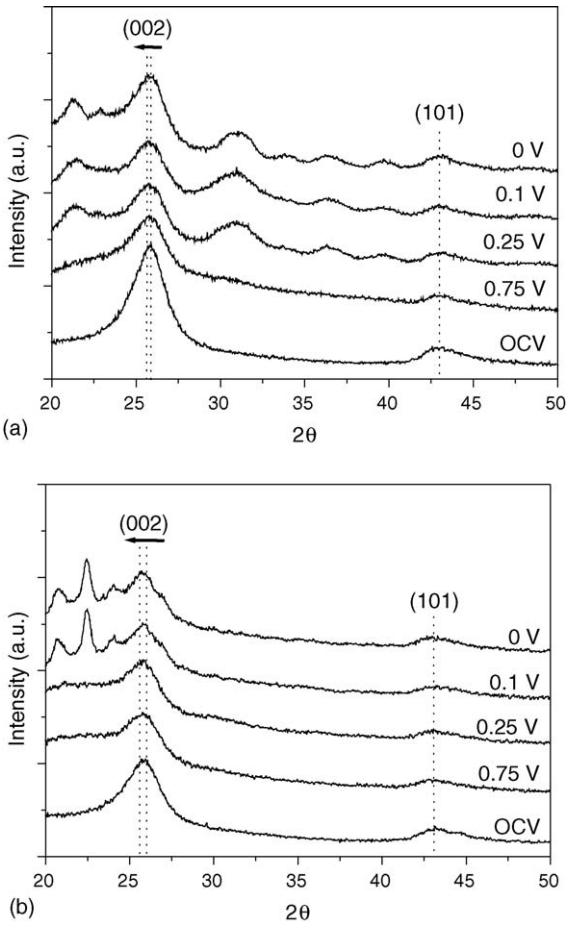

Fig. 9. X-rays diffraction peaks at different voltages stages during first discharge (insertion) of (a) purified MWNTs and (b) MWNTs ball-milled for 60 min (other peaks are unknown). All samples were contained in a glass capillary tube in an argon filled glove box and then measured using Cu Kα of 1.54 Å at 40 kV in the transmission mode.

samples, although the surface area of the ball-milled MWNTs increases with ball-milling time.

Following the voltage plateau at 0.8 V, the voltage declines with a sloping profile, and the majority of Li ions are inserted into MWNTs below 0.25 V. No voltage plateau is observed below 0.25 V in the charge–discharge curves and indicates the absence of a well-defined insertion staging phenomena in both the purified MWNTs and the ball-milled MWNTs. A sloping profile of the voltage below 0.25 V is also observed in amorphous carbonaceous materials [17,18].

It has been reported that for MWNTs of perfect structure with closed ends Li ions cannot be inserted between the graphene layers and also into the inner core (the cavities in centers of MWNTs) through the carbon pentagons and hexagons. For MWNTs with opened ends and lateral defects, however, Li ions can be inserted between the graphene layers through the lateral defects [1] and the opened ends, and also inserted into the inner core through the open ends [5]. In addition, Li ions are doped on to the surface of MWNTs and also at the edge of the graphene layers [17,18]. The insertion and extraction of Li ions between the graphene layers occur reversibly, and proceed with a low voltage profile in the charge–discharge curves [16–18]. To examine the insertion of Li ions between the graphene layers of the purified MWNTs and the ball-milled MWNTs, XRD experiments were performed on the purified MWNTs and the ball-milled MWNTs at different voltage stages during the first discharge process. The results are presented in Fig. 9. From the (0 0 2) diffraction peaks at the open-circuit voltage (OCV) for the purified MWNTs as well as the ball-milled MWNTs, the $d(0\,0\,2)$ spacing or the distance between the graphene layers is calculated to be 3.44 and 3.43 Å, respectively. As Li ions are inserted into the purified MWNTs and the ball-milled MWNTs, the (0 0 2) diffraction peaks shifted slightly to lower angles, i.e., the $d(0\,0\,2)$ spacing of MWNTs discharged to 0 V increased to 3.46 Å for the purified MWNTs and 3.47 Å for the ball-milled MWNTs. The increase in the $d(0\,0\,2)$ spacing for the ball-milled MWNTs with Li insertion is larger than that for the purified MWNTs. This suggests that more Li ions are inserted easily between the graphene layers in the ball-milled MWNTs due to increase in the open ends formed by fracture of the individual MWNTs during ball-milling.

It is evident from the large voltage hysteresis in the charge–discharge curve shown in Fig. 6 that most of the Li ions are inserted below 0.25 V in the discharge process, but are extracted almost uniformly between 0 and 3 V. This means that the extraction of Li ions from ball-milled MWNTs is greatly hindered. Such a large hysteresis was previously observed for MWNTs [1–6] and SWNTs [7–11], and for ball-milled sugar carbons [13] and soft carbons containing a substantial amount

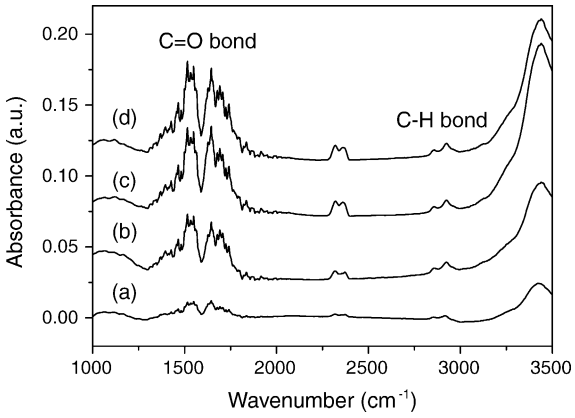

Fig. 10. FT-IR spectra in absorbance mode of (a) purified MWNTs and MWNTs ball-milled for (b) 30; (c) 60 and (d) 120 min.

of hydrogen [19]. This feature is generally attributed to bonding changes in the host, or activated process such as the formation of C–H–Li [19,20] or C–O–Li [21] species [2,4,8]. Surface functional groups containing C–O and C–H bonds for the purified MWNTs and the ball-milled MWNTs are indicated by the FT-IR spectra shown in Fig. 10. These C=O and C–H bonds were found to be carbonyl (C=O) and carboxyl (−COOH) groups [6,16,22–26]. The surface functional groups were chemically bonded to the carbons at the edges of fractured graphene layers by the ball-milling. It is evident from the change in the peak intensity associated with each bond in Figs. 5 and 10 that the amount of the surface functional groups formed on MWNTs increases with ball-milling time. Since the contents of hydrogen and oxygen in the surface functional groups increase with the increase in ball-milling time, as shown in Table 1, a large voltage hysteresis is observed in the ball-milled MWNTs.

The exact mechanism for the enhanced C_{rev} in the ball-milled MWNTs compared with that in the purified MWNTs is not yet clear. Several models have been reported to account for the excess C_{rev} observed in other carbonaceous materials. These include the formation of Li multi-layers and Li_2 covalent molecules on graphene layers, the formation of C–H–Li bonds in soft carbons. The filling of micro-cavities and the adsorption of Li ions on both sides of isolated graphene layers [16–18]. In the ball-milled MWNTs, the edges of graphene layers are formed by fracture of the individual MWNTs during the ball-milling, and increase with the ball-milling time. Also, the surface functional groups are chemically bonded to the carbons at the edges of fractured graphene layers of the ball-milled MWNTs.

Table 1
Contents of hydrogen and oxygen in surface functional groups of purified MWNTs and ball-milled MWNTs as function of ball-milling time (measured by elemental analysis)

	Hydrogen (at.%)	Oxygen (at.%)
Purified	4.9185	0.6937
Ball-milled for 30 min	5.2610	5.4175
Ball-milled for 60 min	5.6594	6.0647
Ball-milled for 120 min	6.5993	8.0720

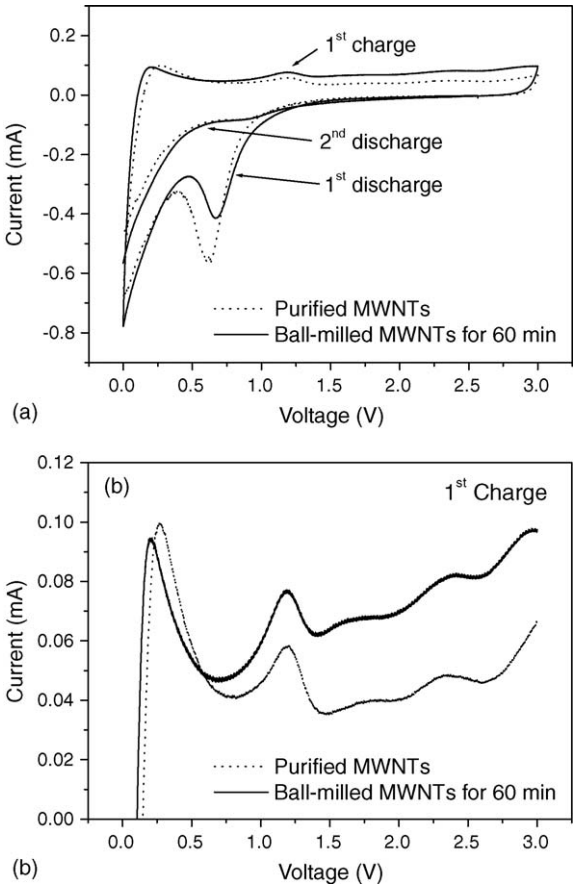

Fig. 11. (a) Cyclic voltammograms for purified MWNTs and MWNTs ball-milled for 60 min; (b) first charge cyclic voltammograms. Li/MWNTs cells scanned at a constant rate of 0.1 mV s^{-1} between 0 and 3 V.

Therefore, these features of the ball-milled MWNTs facilitate the insertion of Li ions and enhance the C_{rev}. From the change in C_{rev} and C_{irr} of ball-milled MWNTs (Fig. 7), it is evident that the enhanced C_{rev} is due to a continuous decrease in the C_{irr} because the MWNTs develop a densely-packed structure on ball-milling. The reduction of C_{rev} with further ball-milling is attributed to a increase in the disordered/amorphous carbon at the expense of the ball-milled MWNTs.

3.3. Cyclic voltammetry behaviour of ball-milled MWNTs

Cyclic voltammograms for purified MWNTs and MWNTs ball-milled 60 min are given in Fig. 11. The curves for all the samples clearly show peaks that correspond to the insertion and extraction of Li ions. Peaks at 0.8 V appear in the first discharge (Fig. 11(a)) and correspond to the voltage plateau at 0.8 V in the discharge curve shown in Fig. 6. These are presumably due to an irreversible reaction in the Li insertion into MWNTs [5,24]. The integrated peak area around 0.8 V for the ball-milled MWNTs is smaller than that for the purified MWNTs, which indicates that the amount of Li ions for the formation of the SEI in the ball-milled MWNTs is smaller than that in the purified MWNTs due to the densely-packed structure of the ball-milled MWNTs by fracture and flattening of the individual MWNTs with ball-

milling. Therefore, the C_{irr} of the ball-milled MWNTs is found to be less than that of the purified MWNTs.

In the first discharge cyclic voltammograms (Fig. 11(a)), the peak at 0.8 V for the purified MWNTs is shifted to 0.9 V for the ball-milled MWNTs. This suggests that Li ions are inserted into the inner core of the ball-milled MWNTs through the open ends. On the other hand, the extraction of Li ions from the inner core is greatly hindered due to the strong tendency of MWNTs to accumulate Li ions [5]. It appears that the insertion of Li ions into the inner core of the ball-milled MWNTs is facilitated more than that of the purified MWNTs due to the shortened length of the ball-milled MWNTs and this results in an enhanced C_{rev} for the ball-milled MWNTs.

In the first charge cyclic voltammograms (Fig. 11(b)), peaks around 0.2, 1.25 and 2.25 V are observed for both purified MWNTs and ball-milled MWNTs. The peaks around 0.2 and 1.25 V are attributed to the extraction of Li ions between the graphene layers and from the inner core of the purified MWNTs and the ball-milled MWNTs, respectively. The extraction of Li ions between the graphene layers and from the inner core of the ball-milled MWNTs appears to be easier than in the case of purified MWNTs due to the shortened length of the ball-milled MWNTs. Also, the peaks around 2.25 V are attributed to the extraction of Li ions bonded to the surface functional groups in the purified MWNTs and the ball-milled MWNTs, but the amount of extracted Li ions from the surface functional groups in the ball-milled MWNTs is larger than that in the purified MWNTs due to increase in the contents of hydrogen and oxygen in the surface functional groups by the ball-milling, as shown in Table 1. It appears that the excess C_{rev} of the ball-milled MWNTs is due to the excess extraction of Li ions from the inner core (around 1.25 V peak) and the surface functional groups (around 2.25 V peak) of the ball-milled MWNTs.

3.4. Cycle-life behaviour of ball-milled MWNTs

The reversible capacity (C_{rev}) and coulombic efficiency of purified MWNTs and MWNTs ball-milled for 60 min as a function of cycle number are shown in Fig. 12. The purified MWNTs and the ball-milled MWNTs present almost uniform cycle capacity, e.g., the purified MWNTs maintain 89% (311 mAh g^{-1}) of their initial capacity (351 mAh g^{-1}) and the ball-milled MWNTs maintain 96% (616 mAh g^{-1}) of their initial capacity (641 mAh g^{-1}) after 50 cycles, see Fig. 12(a).

The coulombic efficiency of the ball-milled MWNTs is higher than that of the purified MWNTs (Fig. 12(b)). This suggests that most of the SEI in the ball-milled MWNTs is formed simultaneously on all the surfaces during the initial charge–discharge cycling, whereas in purified MWNTs only a small amount of the SEI is formed continuously. Therefore, the insertion and extraction of Li ions into/from the densely-packed structure of the ball-milled MWNTs is more reversible than that into/from the porous structure of the purified MWNTs. Nevertheless, the coulombic efficiency of the purified MWNTs is almost 100% after completion of the formation of the SEI on the surface during charge–discharge cycling.

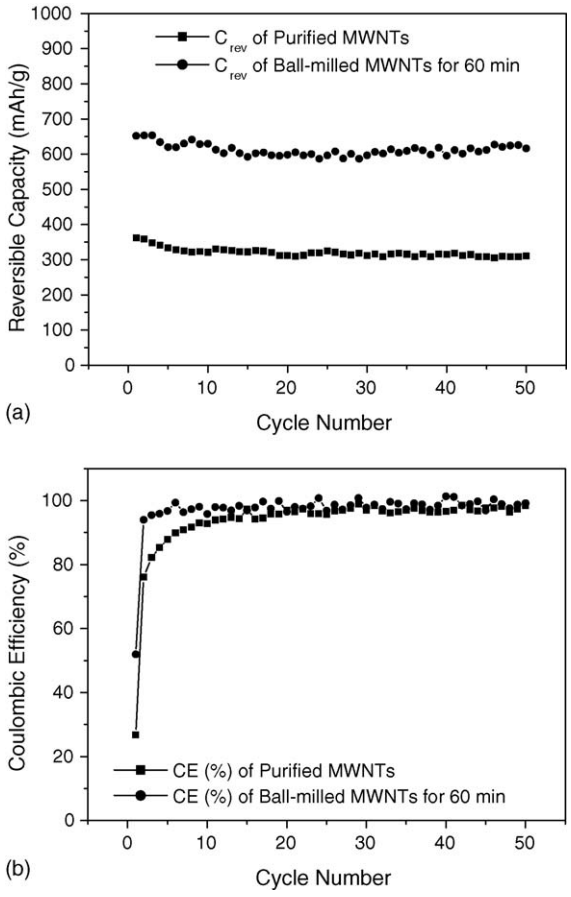

Fig. 12. (a) Reversible capacity and (b) coulombic efficiency of purified MWNTs and MWNTs ball-milled for 60 min as a function of cycle number.

4. Conclusions

1. The C_{rev} of ball-milled MWNTs increases with increasing ball-milling time to 60 min., namely, from 351 mAh g^{-1} ($Li_{0.9}C_6$) for the purified MWNTs to 641 mAh g^{-1} ($Li_{1.7}C_6$) for the ball-milled MWNTs. For the ball-milled MWNTs, the edges of graphene layers formed by fracturing and the surface functional groups chemically bonded to the edges of fractured graphene layers facilitate the insertion of Li ions into the MWNTs, and hence enhanced the C_{rev}.
2. The extraction of Li ions from the ball-milled MWNTs appears to be easier than that from the purified MWNTs due to the shortened length of the former. The undesirable C_{irr} decreases continuously with increase in ball-milling time, i.e., from 1012 mAh g^{-1} ($Li_{2.7}C_6$) for purified MWNTs to 518 mAh g^{-1} ($Li_{1.4}C_6$) for MWNTs ball-milled for 2 h. It is considered that the reduction in C_{irr} for ball-milled MWNTs is due to an increase in the densely-packed structure of MWNTs by the ball-milling.
3. The increase in C_{rev} and the decrease in C_{irr} of the ball-milled samples results in an increase in the coulombic efficiency from 25% for the purified sample to 50% for the ball-milled sample. In addition, ball-milled samples exhibit more stable cycle capacities than purified samples during the charge–discharge cycling.

References

[1] G. Maurin, C. Bousquet, F. Henn, P. Bernier, R. Almairac, B. Simon, Chem. Phys. Lett. 312 (1999) 14–18.
[2] G.T. Wu, C.S. Wang, X.B. Zhang, H.S. Yang, Z.F. Qi, P.M. He, et al., J. Electrochem. Soc. 146 (5) (1999) 1696–1701.
[3] T. Ishihara, A. Kawahara, H. Nishiguchi, M. Yoshio, Y. Takita, J. Power Sources 97–98 (2001) 129–132.
[4] E. Frackowiak, S. Gautier, H. Gaucher, S. Bonnamy, F. Beguin, Carbon 37 (1999) 61–69.
[5] Z.H. Yang, H.Q. Wu, Solid State Ionics 143 (2001) 173–180.
[6] T.P. Kumar, A.M. Stephan, P. Thayananth, V. Subramanian, S. Gopukumar, N.G. Renganathan, et al., J. Power Sources 97–98 (2001) 118–121.
[7] B. Gao, A. Kleinhammes, X.P. Tang, C. Bower, L. Fleming, Y. Wu, et al., Chem. Phys. Lett. 307 (1999) 153–157.
[8] A.S. Claye, J.E. Fischer, C.B. Huffman, A.G. Rinzler, R.E. Smalley, J. Electrochem. Soc. 147 (8) (2000) 2845–2852.
[9] B. Gao, C. Bower, J.D. Lorentzen, L. Fleming, A. Kleinhammes, X.P. Tang, et al., Chem. Phys. Lett. 327 (2000) 69–75.
[10] H. Shimoda, B. Gao, X.P. Tang, A. Kleinhammes, L. Fleming, Y. Wu, et al., Physica B 323 (2002) 133–134.
[11] H. Shimoda, B. Gao, X.P. Tang, A. Kleinhammes, L. Fleming, Y. Wu, et al., Phys. Rev. Lett. 88 (1) (2002) 15502.
[12] J.S. Benjamin, Met. Powder Rep. 45 (1990) 122–127.
[13] W. Xing, R.A. Dunlap, J.R. Dahn, J. Electrochem. Soc. 145 (1) (1998) 62–70.
[14] B. Zheng, Y. Li, J. Liu, Appl. Phys. A 74 (2002) 345–348.
[15] J.Y. Eom, H.S. Kwon, J. Liu, O. Zhou, Carbon 42 (2004) 2589–2596.
[16] K. Kinoshita, Carbon: Electrochemical and Physicochemical Properties, Wiley, NY, USA, 1988, pp. 293–387.
[17] J.O. Besenhard, Handbook of Battery Materials, Wiley, Weinheim, 1999, pp. 231–244.
[18] T. Osaka, M. Datta, Energy Storage Systems for Electronics, Gordon, Singapore, 2000, pp. 193–251.
[19] J.R. Dahn, T. Zheng, Y. Liu, J.S. Xue, Science 270 (1995) 590–593.
[20] P. Zhou, P. Papanek, R. Lee, J.E. Fischer, J. Electrochem. Soc. 144 (1997) 1744–1750.
[21] M.D. Levi, E.A. Levi, D. Aurbach, J. Electroanal. Chem. 421 (1997) 89–97.
[22] J. Liu, A.G. Rinzler, H. Dai, J.H. Hafner, A.R. Bradley, P.J. Boul, et al., Science 280 (1998) 1253–1256.
[23] T. Saito, K. Matsushige, K. Tanaka, Physica B 323 (2002) 280–283.
[24] W. Xing, J.R. Dahn, J. Electrochem. Soc. 144 (4) (1997) 1195–1201.
[25] E. Peled, C. Menachem, D.B. Tow, A. Melman, J. Electrochem. Soc. 143 (1) (1996) L4–L7.
[26] Y.E. Eli, V.R. Koch, J. Electrochem. Soc. 144 (9) (1997) 2968–2973.